The Near-Earth Space Radiation Environment During Solar Cycle 25: Consequences for the Alabama Burst Energetics eXplorer

Michael Halvorson
University of Alabama in Huntsville, Complex Systems Integration Lab
Wernher von Braun Research Hall, 301 Sparkman Drive, Huntsville, AL 35899; 334-300-8131
mch0043@uah.edu

Tyler Tolbert, Kody Ehlers, Ross Anderson, Chris Howell, Keller Stallings
Auburn University, 354 War Eagle Way, Auburn, AL 36849
twt0009@auburn.edu

ABSTRACT

The Alabama Burst Energetics eXplorer (ABEX) is a 12U mission to enhance the detection of low energy Gamma Ray Burst (GRB) components and provide improved, rapid localization of short GRBs for multiwavelength follow up via GRB measurements outside the Van Allen Belts (VAB). The ABEX launch date is Q4 2024 during the peak of solar cycle 25; the ABEX science orbit is 300 km perigee by 60,000 km apogee with an inclination of 27°. This orbit defines distinct radiation environments in Low Earth Orbit, crossing the VABs, performing science operations outside the VABs, and Coronal Mass Ejection (CME) conditions. Numerical trajectory data was generated in AGI's Systems Tool Kit and provided to the Space Environment Information System (SPENVIS). VAB trapped particle, Solar Energetic Particle, and Galactic Cosmic Ray particle fluxes were determined for the ABEX orbit. Empirical fits for Total Ionizing Dose are provided per particle source. Solar cell degradation as a function of Non-Ionizing Energy Loss was calculated per coverglass thickness with mass implications. Charged Particle Heating is characterized in a full thermal radiation model. Single Event Effects and surface charging are not discussed in the context of particle flux.

NOMENCLATURE

$\boldsymbol{aF}$	= Albedo Factor
C	= MC-SCREAM Unitless Constant
D_{Orbit}	= Satellite Altitude
D_{Sun}	= Distance to Center of the Sun
D_x	= MC-SCREAM Mass Stopping Power
E	= Particle Energy
E_{Max}	= Max Energy
E_{Min}	= Min Energy
f_s	= Shadow Fraction
I_{Pmax}	= Max Current at Max Power Point
I_{sc}	= Short Circuit Current
K_E	= Conversion Factor, MeV to Joule
K_t	= Conversion Factor, Years to Minutes
m_{cg}	= Mass of Coverglass
n	= MC-SCREAM Electron Damage Coefficient
n_{CME}	= Coronal Mass Ejections per Year
P_{Max}	= Max Power Point
$P(CME)$	= Probability of CME
Q''_{Albedo}	= Planetary Albedo Heat Flux of Earth
Q''_{CPH}	= Charged Particle Heat flux
$Q''_{Earth,Surf}$	= Emissive Heat Flux from Earth Surface
$Q''_{Emission}$	= Emissive Heat Flux from Earth
Q''_{FMH}	= Free Molecular Heat Flux
Q''_{Solar}	= Direct Solar Heat Flux
$Q''_{Solar,Surf}$	= Heat Flux at Sun Surface
Q'_{sp}	= Specific Power
R_{Earth}	= Radius of Earth
R_{Sun}	= Radius of Sun
s_{Pen}	= Penetration Depth
TID_{GCR}	= Total Ionizing Dose, GCR
$TID_{SEP,p}$	= Total Ionizing Dose, SEP Protons
TID_{Total}	= Total Ionizing Dose, All Sources
$TID_{VAB,e}$	= Total Ionizing Dose, VAB Electrons
$TID_{VAB,p}$	= Total Ionizing Dose, VAB Protons
t_{Shield}	= Aluminum Shield Thickness
V	= Spacecraft Velocity
$\vec{V}_{E,cs}$	= Earth to Satellite Vector
$\vec{V}_{E,S}$	= Earth to Sun Vector
V_{oc}	= Open Circuit Voltage
V_{Pmax}	= Max Voltage at Max Power Point
α_t	= Thermal Accommodation Coefficient
Δt	= Discretized Time Step
ξ	= Solar Zenith Angle
η_{Cell}	= Solar Cell Efficiency
ρ_{Atm}	= Atmospheric Density
ρ_{Mat}	= Material Density
$\varphi(t,x)$	= Particle Intensity

INTRODUCTION

ABEX Foundations

The Alabama Burst Energetics eXplorer (ABEX) is the flagship mission of the Alabama CubeSat Initiative's (ACSI) statewide student spacecraft design program funded by the Alabama Space Grant Consortium (ASGC). The ABEX university cohort includes the University of Alabama, University of South Alabama, Auburn University, the University of Alabama in Huntsville, Tuskegee University, and the University of Alabama in Birmingham. Over 150 undergraduates have been taught space system design and operation; further details are available[1]. Program educational value is derived in part from in-house design of principal subsystems, including the On-Board Computer (OBC), Software-Defined Radio (SDR), science instruments, and Electrical Power System (EPS). Qualification of in-house subsystems to radiation exposure is challenging for university programs, so a thorough understanding of the Space Radiation Environment (SRE) and its effects on ABEX must be analytically determined in lieu of empirical component testing. The present work describes both thermal and corpuscular radiation environments consequential to circuitry, software, and shielding design, but circuit and software-level mitigation strategies are not discussed.

Mission Background

The ABEX science mission will enhance the detection of low energy Gamma Ray Burst (GRB) components and provide improved, rapid localization of short GRBs for multiwavelength follow up. ABEX instrumentation consists of a suite of X-ray and gamma-ray detectors that measure relative energies of GRB prompt emission. The goal is to search for low energy spectral breaks and possible thermal components in a commonly undetected portion of the prompt emission spectrum. ABEX will be deployed from a super-synchronous launch vehicle trajectory in Q4 2024 and traverse a highly eccentric orbit from 300 km perigee to 60,000 km apogee. From this vantage point outside the Van Allen Belts (VAB) ABEX will measure wavefront timing between other LEO-based gamma ray missions to localize GRBs in the sky. The localization goal is to provide a timing annulus under a few degrees within 8 to 12 hours from a burst trigger. The satellite will feature an initial inclination of 27°; science operations duration success is defined as 1 year. A Systems Tool Kit (STK) model of the science orbit is shown in Figure 1.

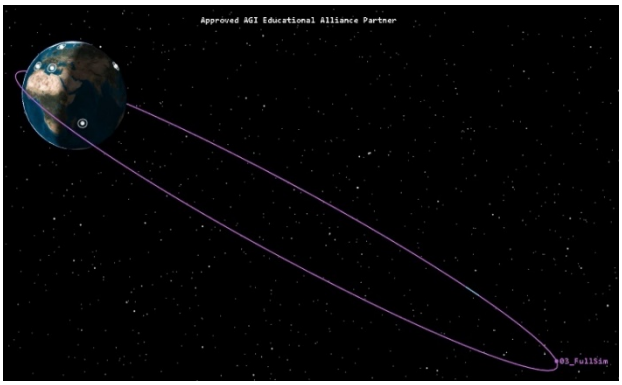

Figure 1: ABEX Orbit on May 3rd, 2025, 300 km Perigee x 60,000 km Apogee, Inclination 27°

Space Radiation Environment Preface

Space is radioactive. Predicting radiation type, energy level, and interaction mechanism with a target material such as spacecraft chassis material or dedicated radiation shielding can assist in characterizing electronics-level exposure assessment parameters such as Total Ionizing Dose (TID), Non-Ionizing Energy Loss (NIEL), Single Event Effect (SEE) rates, Charged Particle Heating (CPH), and spacecraft surface charging. Three particle sources are of interest for basic SRE determination: Solar Energetic Particles (SEP), Galactic Cosmic Rays (GCR), and VAB trapped particles[2].

SEPs are particles resulting from solar activity such as solar flares and Coronal Mass Ejections (CME); they are primarily comprised of protons but also contain heavy ions, electrons, gamma rays, and X-rays depending on the type and intensity of the initiating event. Worst-case proton energies such as those seen in the Halloween event of 2003 were measured up to 600 MeV in Geosynchronous Equatorial Orbit (GEO), but particle fluxes above 400 MeV are low for many CMEs[2]. Worst-case CME heavy ion energies were measured above 1,000 MeV in GEO for the October 20, 1989 event, but differential fluxes for all species above He at that energy were less than 1e-7 pfu[2]. A proton energy cutoff of 400 MeV has been selected for SEPs, and increased SEP model confidence levels are used to characterize highly energetic CMEs. SEP heavy ions including alpha particles are not considered for CPH due to their relatively low flux contribution. In general, CME particle sources are low-to-moderate energy, high flux, and locally isotropic in space.

GCRs are comprised of heavy ions ranging from hydrogen to uranium; they are lower flux and higher energy than SEPs. As with SEPs, particle flux decreases with increasing atomic number, and particle energy

increases with increasing atomic number. Particle energies can reach up to 10^{20} MeV[2]. H and He represent ~99% of GCR flux, and the high energy, low flux nature of GCR causes SEEs more so than an increase in TID, CPH, NIEL, or surface charging. The energy cutoff for CPH determination purposes in the present work is 10,000 MeV as particle fluxes above that energy are negligibly low for all metrics other than SEE rates. GCR H flux can reach as high as 1e3 pfu but is commonly closer to 1e1 pfu. GCR flux varies approximately 10% between high at solar minimum and low at solar maximum, a process known as the Forbush effect[3].

There are usually[4] two VABs: an inner belt comprised primarily of protons that also contains electrons and ions and an outer belt comprised primarily of electrons that also contains protons and ions. Only protons up to 400 MeV and electrons up to 7 MeV are considered for trapped particle CPH and TID; ions are not considered.

ABEX will traverse the VABs twice per orbit, encounter corpuscular radiation from SEPs and GCR, and receive electromagnetic radiation from the Sun. All sources and radiation types must be analyzed for spacecraft interactions; the present work will detail CPH, NIEL, TID, and electromagnetic radiation culminating in a spacecraft thermal radiation environment. To model corpuscular radiation, STK-generated trajectory data for the ABEX science orbit was provided to the Space Environment Information System (SPENVIS). STK-generated orbit data was also an input to a MATLAB model determining on-orbit heat flux from first principles. All radiation data provided in this work is specific to ABEX orbit data; apogee and perigee data change slightly over time.

Thermal heat sources discussed include direct solar radiation, planetary albedo, planetary emission, free molecular heating (FMH), and CPH[5]. Direct solar heating is an integration of Planck's blackbody radiation equation at 5,780 K and is varied as a function of spacecraft distance. Eclipse conditions are calculated and affect both direct solar thermal radiation and SEP flux. Planetary albedo heating manifests as direct solar radiation reflecting off a planetary body. Planetary albedo is directly related to orbit position; the spacecraft albedo model accounts for orbit position and eclipse conditions as detailed in Rickman[6] and expanded in Halvorson[7]. Planetary emission heating is a simple integration of the Planck blackbody radiation equation. Free molecular heating is caused by atmospheric drag on the satellite and is dependent on both spacecraft velocity and atmospheric density. Charged particle heating occurs when a spacecraft encounters energetic particles trapped in the VABs, from extrasolar origin as GCR, or emitted from the Sun as SEPs during CMEs or solar wind during quiet Sun activity. These particles deposit energy to the spacecraft surface resulting in a thermal load. Operational internal heat generation as a result of component power conversion efficiencies and intentional heat generation via heater operation are not characterized in this work; required heater wattages and radiator areas may be determined once internal heating, surface areas, absorptivities, and emissivities are factored into a spacecraft's thermal model.

SUN CONDITIONS

Solar activity is cyclical and operates on an ~11-year cycle, with peak solar activity (solar maximum) typically occurring around the 4th or 5th year of a solar cycle[8]. Solar Cycle 25 began in September 2020[9], which places predicted solar maximum during the ABEX mission in 2024-2025. Solar maximum is colloquially defined by the number of sunspots on the Sun's surface, and CME initiation as flares is directly related to sunspot structure[10]. During solar maximum, the Sun either emits nominal radiation during quiet Sun periods or erupts charged particles as CMEs travelling at velocities ranging from 250 km/s to nearly 3,000 km/s[11].

CMEs are measured using a coronagraph such as the Large Angle and Spectrometric Coronagraph (LASCO) instrument on NASA's Solar and Heliospheric Observatory (SOHO). For solar cycle 25 CME frequency prediction, historical data collected by LASCO during Solar Cycle 23 is used as a basis for number of CMEs that will be experienced during the ABEX mission and can be seen in Figure 2. Taking a 5-year average centered around 2003 results in an average of 34.8 halo CMEs. Applying a 20% margin to this value to account for directional, non-halo CMEs yields 41.76 or 42 CMEs. This value is used for the number of predicted CMEs and applied probabilistically in the ABEX radiation model.

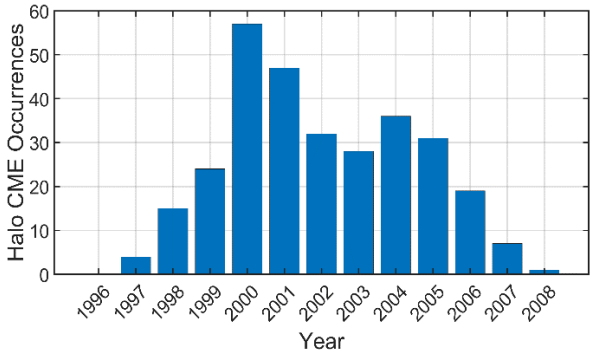

Figure 2: Halo CMEs During Solar Cycle 23 (May 1996 – Jan 2008)

There is unsubstantiated speculation that both the solar cycle and energetic solar surface activity are tied to the motion of the solar system barycenter, which is dominated by the gravity of Jupiter and Saturn[12]. When the third derivative of the barycenter position is at local maxima, this "stirs" the solar mantle resulting in sunspots and CMEs. If this speculation is deemed plausible, ABEX will predict barycenter third derivative maxima and plan to enter safety states during those dates. A recent paper asserts solar activity may cause terrestrial earthquakes[13] when it may in fact be the barycenter jerk causing both energetic solar activity and earthquakes. Community analysis is warranted.

SPACE ENVIRONMENT INFORMATION SYSTEM

SPENVIS is a web-based interactive tool providing engineers and scientists access to space environment data and its effects on space systems. SPENVIS contains several models that have been developed by agencies around the world using a combination of empirical data and probabilistic modeling. SPENVIS requires a spacecraft orbit which can either be generated internally or via software such as STK and uploaded to SPENVIS. All particle data in the present work was generated in SPENVIS and is specific to worst-case scenarios for spacecraft operating in this environment. Fluxes should be considered limiting cases, not nominal flux conditions.

VAN ALLEN BELT TRAPPED PARTICLES

The magnetosphere is a magnetized shield that both deflects charged particles away from Earth and traps them in toroidal regions called the Van Allen Belts (VAB). The inner belt consists primarily of protons while the outer belt consists primarily of electrons. Both the inner and outer VABs were accounted for in ABEX's analysis with trapped protons and trapped electrons analyzed separately. Protons in the VABs range from 0.1 MeV to 400 MeV, and electrons in the VABs range from 0.01 to 7 MeV[14]. Figure 3 depicts the two main VABs (inner and outer).

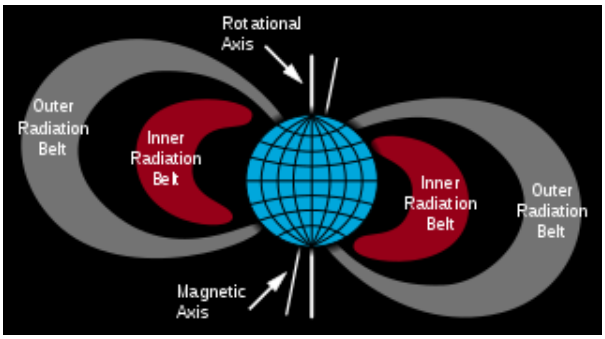

Figure 3: The Van Allen Belts[15]

The VABs are temporally variable in both size and composition. NASA describes the first VAB existing between ~1,600 km and ~12,800 km and the second VAB existing between ~19,300 km and ~40,000 km[15]. These numbers can be taken as a first order estimate, but obtaining a set thickness for the VABs is impractical because thickness is dependent upon solar conditions and which side of Earth a satellite is on relative to the Sun. The VABs between the Sun and Earth are thinner than the VABs behind Earth relative to the Sun due to solar radiation pressure; VABs can extend out to 10 Earth radii or farther. ABEX considers the second VAB outer boundary to be 52,000 km for modeling purposes.

It is preferable for spacecraft to operate below the first VAB, such as the International Space Station at 419 km, or in the "slot" between the two VABs. For spacecraft with operational capabilities dependent on radiation-induced noise, such as the science instrumentation on ABEX, a more realistic approach is to empirically determine the VAB structure. Phase 3 of the ABEX mission is science commissioning wherein the science instrument will obtain baseline in-situ radiation noise measurements to be removed from GRB data in post-processing. If the instruments are powered-on during an outbound VAB passing near 35,000 km, the instruments can take measurements of VAB-induced noise. The altitude threshold at which VABs are no longer considered pertinent to operation can be empirically determined in this manner, and a software update can be uplinked commanding the satellite to remain in a safety state outbound from 1,600 km to the VAB threshold altitude. With operational altitudes determined and science instrumentation deemed functional, ABEX can proceed to mission phase 4, science operations. The VAB threshold determination procedure may be repeated periodically as needed.

Peak integral fluxes for both protons and electrons in the relevant VAB energy ranges were found using the AP8 and AE8 VAB particle models in SPENVIS[14]. Peak fluxes were calculated because worst-case scenarios are pertinent for determining shielding material type, physical location, and thickness, among other non-structural reasons such as SEE rate and TID assessments. AP9 and AE9 models exist[16] that are higher fidelity than AP8 and AE8, but they require Air Force Research Lab approval[17] (or perhaps Space Force approval soon) to obtain. Ideally all new SRE models will become publicly available once the International Radiation Environment Near Earth (IRENE) is launched. Integral flux data sets for VAB protons and electrons are shown in Figures 4 and 5 for the ABEX orbit. Each energy level is plotted for a full orbital period, meaning two lines are shown per energy level representing two VAB crossings.

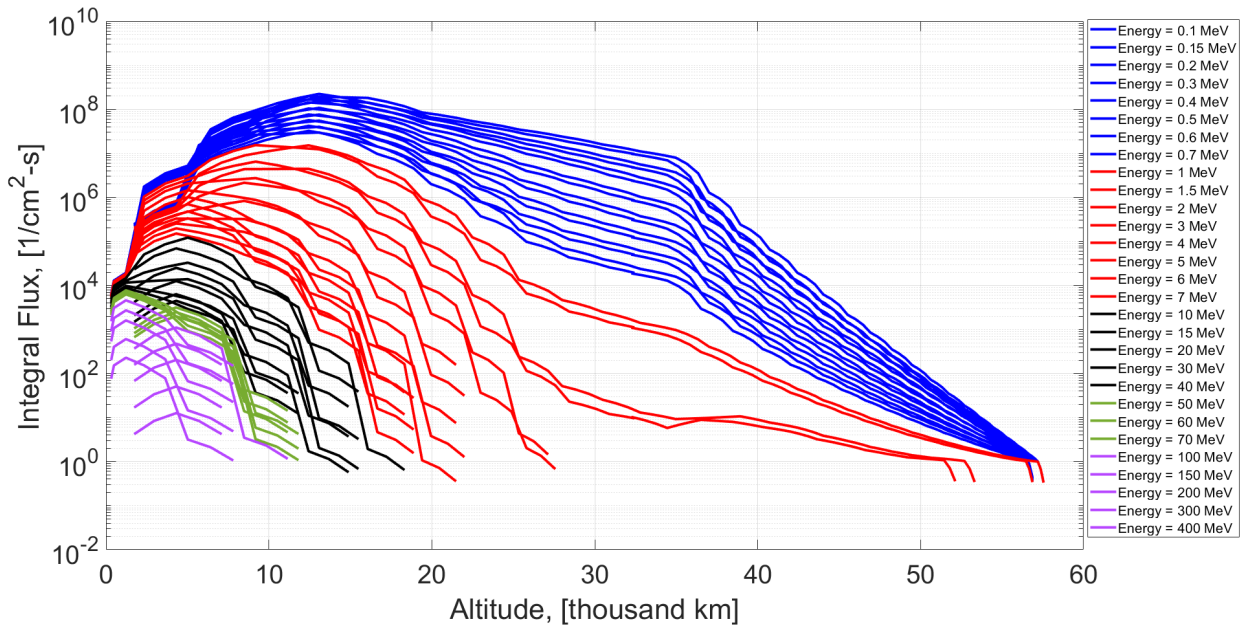

Figure 4: VA B Trapped Proton Integral Flux per Altitude, AP8, no Associated Confidence, Oct 1 2024 – Sep 30 2025

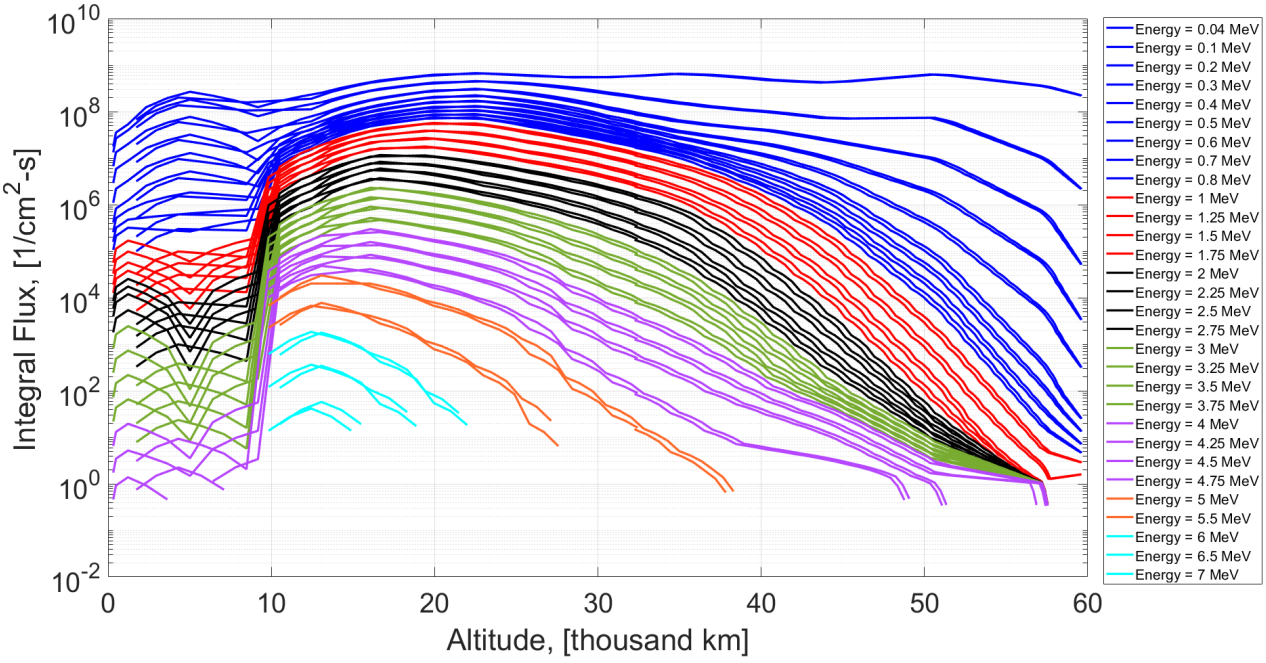

Figure 5: VAB Trapped Electron Integral Flux per Altitude, AE8, 97.73% Confidence, Oct 1 2024 – Sep 30 2025

SOLAR ENERGETIC PARTICLES

SEP-induced effects require considerable attention as ABEX will launch during solar maximum; SEPs cause increased TID, NIEL, SEE rates, surface charging, and CPH. Peak SEP flux conditions inherent to CMEs are of direct importance, but quiet Sun conditions, here meaning solar wind during periods without CMEs, must also be modeled for complete SEP analysis. The Solar Accumulated and Peak Proton and Heavy Ion Radiation Environment (SAPPHIRE) Model was used in SPENVIS to model both quiet Sun and peak CME conditions[18]. Because protons dominate SEP composition above ~1 MeV, shown in Figure 6, only protons were considered for analysis products.

Using SAPPHIRE to determine quiet Sun particle fluxes is challenging. SAPPHIRE peak proton fluxes are output in units of proton/m^2-s-sr-MeV; SAPPHIRE accumulated proton fluence, which includes CMEs for a specified mission duration, are output in units of proton/cm^2 for varied energy levels. SAPPHIRE can only run solar maximum conditions ± 7 years for accumulated fluence, meaning the lowest accumulated fluence condition would be solar maximum plus 7 years. Direct measurements of proton differential flux between 1.8–3.8 MeV were reported in Smith et al.[19] that hover near 1e-1–1e-2 proton/cm^2-s-sr-MeV for non-CME conditions. Applying the Smith et al. values as limiting conditions and assuming isotropic flux incidence, one obtains an integral flux bound of 2.262 protons/cm^2-s for 1.8 MeV, which is the product of 1.8 MeV, 1e-1 proton/cm^2-s-sr-MeV and 4π steradians, and an integral flux bound of 0.478 protons/cm^2-s for 3.8 MeV, which is the product of 3.8 MeV, 1e-2 proton/cm^2-s-sr-MeV and 4π steradians. When SAPPHIRE is used to generate accumulated integral fluence data in proton/cm^2, that data can be divided by mission duration, here one year, to generate integral flux data for comparison to the Smith et al. bounds. Because the SAPPHIRE accumulated values include CMEs, the 1.8 MeV bound is 105.15x higher than the Smith et al. value, and the 3.8 MeV bound is 219.23x higher than the Smith et al. value. The SAPPHIRE accumulated values will be used for the purposes of solar wind particle flux determination for the present work, but it should be noted that these solar wind fluxes may be orders of magnitude higher than actual quiet Sun flux values. CPH analysis discussed later will show the consequences of quiet Sun solar wind flux overestimation are negligible, but flux order of magnitude accuracy is paramount for SEE rates and surface charging effects.

SAPPHIRE input parameters for CME conditions and quiet Sun conditions are provided in Tables 1 and 2. Figure 7 depicts quiet Sun integral flux for protons between 0.1 MeV–400 MeV, and Figure 8 illustrates CME condition integral flux for the same energy range.

Table 1: Quiet Sun Condition SAPPHIRE Input Parameters

Ion Range	H-Fe
Solar Maximum Offset	7 years
Confidence Level (%)	50
Magnetic Shielding	Off above 52,000 km On below 52,000 km

Table 2: CME Condition SAPPHIRE Input Parameters

Ion Range	H-Fe
Solar Maximum Offset	None (mission based)
Confidence Level (%)	97.73
Magnetic Shielding	Off above 52,000 km On below 52,000 km

Thermal spacecraft engineers establish hottest, coldest, and nominal trend heat flux conditions which can be extended to CPH. This is accomplished when modeling GCR and CME SEPs by varying the confidence level. Here, a confidence of 50% represents cold case conditions, 84.1% represents trend case as a 1σ deviation, and 97.73% represents hot case as a 2σ deviation[20]. Integral fluxes for worst-case SEP and GCR conditions are calculated with a confidence level of 97.73%. It is important to note that CME conditions are transient events. They are not instantaneous, but worst-case proton fluxes from major CMEs as described in Figure 8 should not be considered constant proton flux values. For the purposes of CPH determination, discussed at length below, heightened incident proton flux corresponding to a probabilistic CME event is considered to last 12 hours. Speculating, a more likely CME condition profile may be 1 hour at 97.73% confidence, 7 hours at 84.1% confidence, and 4 hours at 50% confidence. Real CMEs have widely varying durations and energy profiles.

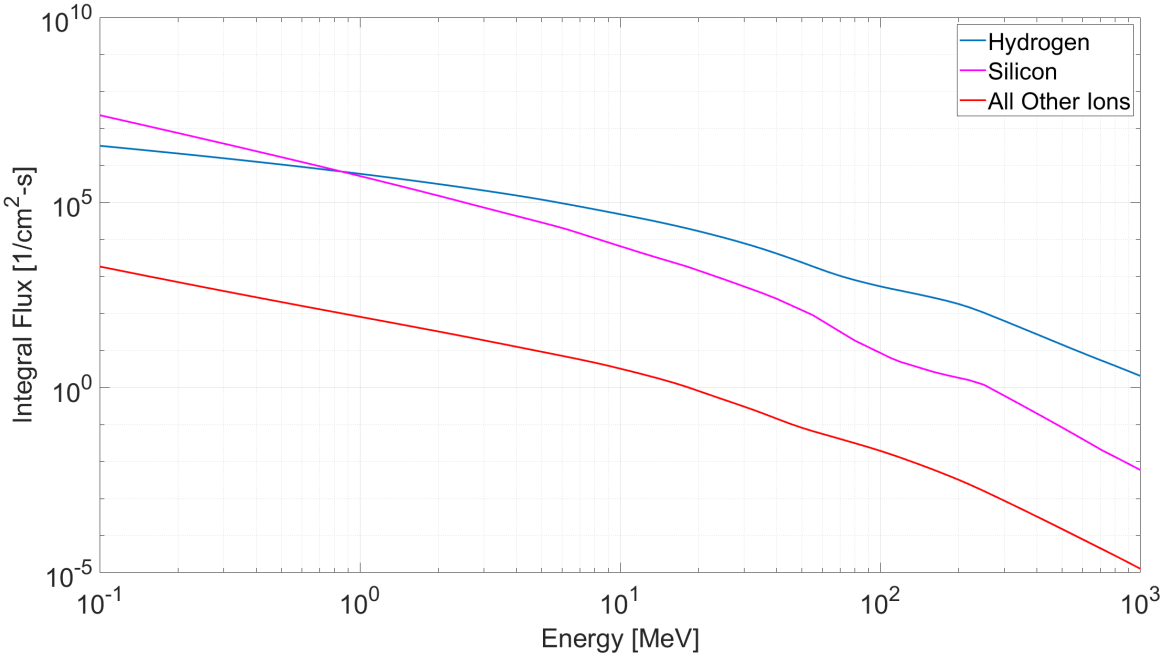

Figure 6: SEP Integral Flux vs. Energy by Species During CME Conditions, SAPPHIRE Peak Model, 97.73% Confidence, Magnetospheric Shielding Off, Oct 1 2024 – Sep 30 2025

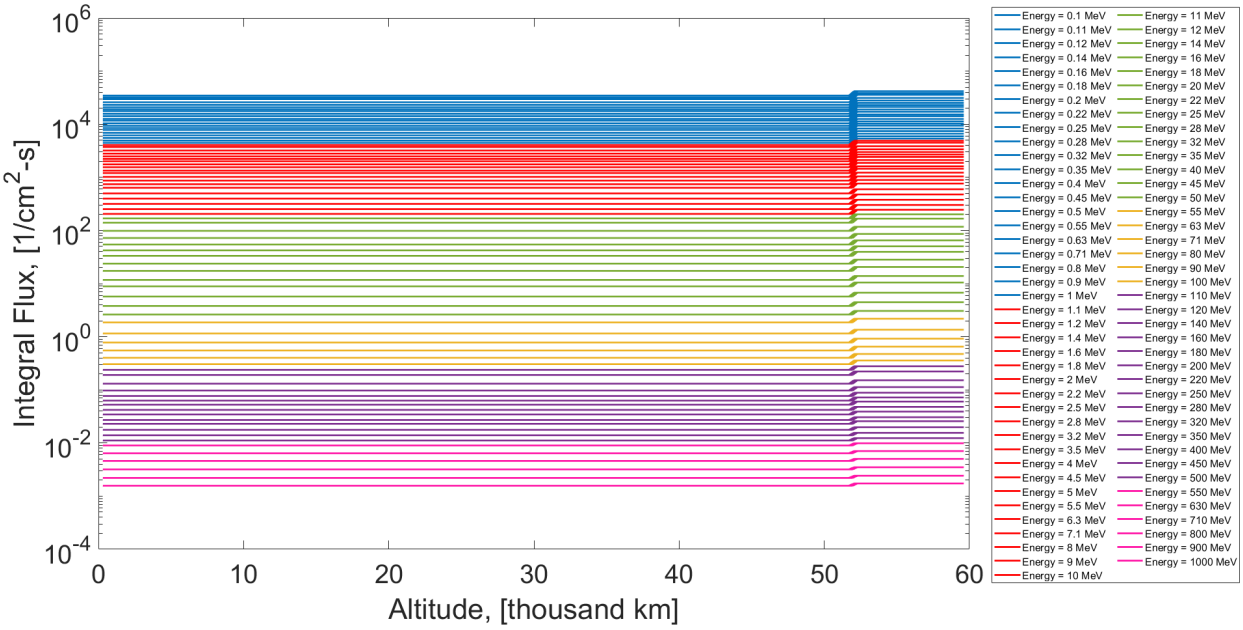

Figure 7: SEP Integral Flux During Quiet Sun Conditions, SAPPHIRE Accumulated Model, 50% Confidence, Magnetospheric Shielding On Below 52,000 km, +7 Year Offset from Mission Epoch

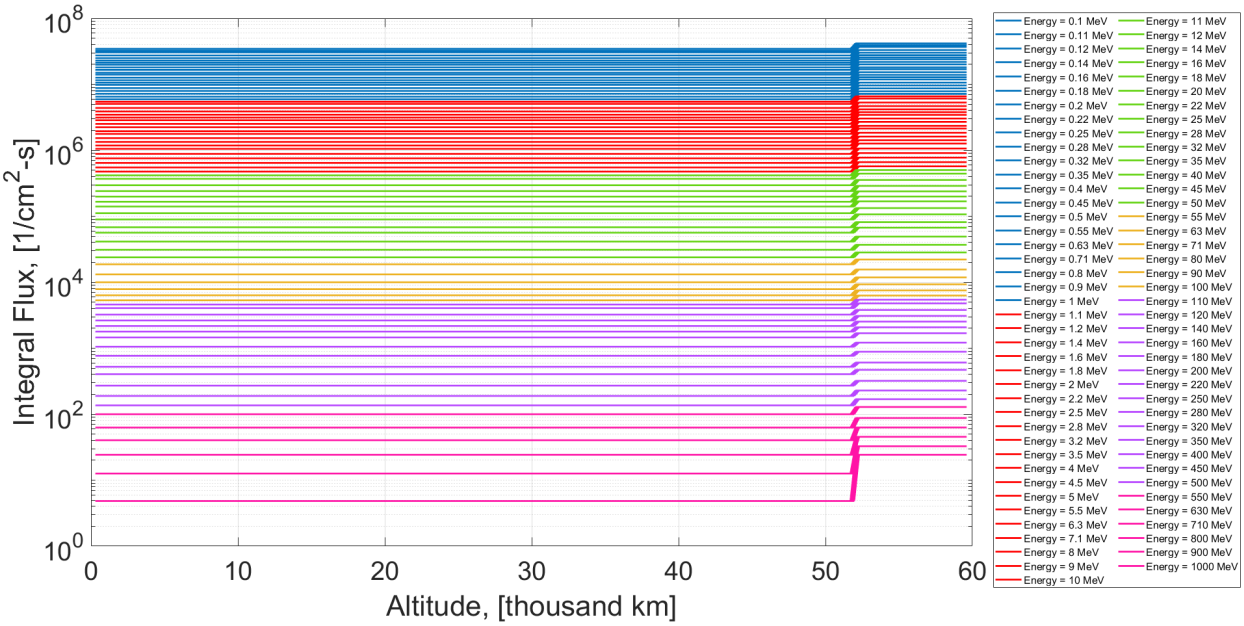

Figure 8: SEP Peak Integral Flux During CME Conditions, SAPPHIRE Peak Model, 97.73% Confidence, Magnetospheric Shielding On Below 52,000 km, Oct 1 2024 – Sep 30 2025

GALACTIC COSMIC RAYS

GCR are energetic charged particles of extrasolar origin[2]; they contribute more to TID and SEE rates than CPH, NIEL, or surface charging due to their higher energy and lower flux. They are not included in provided CPH analyses due to their negligible contributions, but they are included in TID Dose Depth Curve (DDC) empirical fits. Worst-case GCR particle flux is analyzed using the ISO 15390 model with a confidence level of 97.73% (+2σ) and solar activity corresponding to the ABEX mission epoch, described in Table 3. Structural shielding of all GCR particles is practically impossible due to the high particle energies; the particle penetration depth is greater than any feasible satellite shielding thickness. GCR particle flux decreases exponentially for all species above ~1,000 MeV, so extremely high energy GCR particles are rare compared to other, common ionizing radiation sources. Due to the Forbush effect wherein increased solar radiation during solar maximum decreases GCR particle flux values, the absolute worst-case conditions would be the same input conditions as Table 3 but during solar minimum.

Figure 9 details GCR integral flux per energy by species, and the flux decrease above ~1,000 MeV is clearly visible. Species above Fe were not considered due to their negligible flux contributions; the excluded particles would only affect SEE rates. Because H ions (protons) dominate GCR flux trailed loosely by He, only H and He are considered for TID contribution in the DDC

Table 3: GCR ISO 15390 Model Parameters

Ion Range	H-Fe
Confidence Level (%)	97.73
Magnetic Shielding	Off above 52,000 km On below 52,000 km

empirical fits. GCR is not included in CPH. Figure 10 depicts GCR proton and alpha particle integral flux as a function of altitude for various energy levels. Magnetospheric shielding has an appreciable effect on low energy flux, but higher energies are unaffected by the magnetosphere. Proton and α particle integral fluxes at energies between 1 and 100 MeV aggregate strongly near 1.8 per cm^2-s with magnetospheric shielding on.

The hadronic component of GCR is reported in literature as ~87% ionized H or protons, ~12% ionized He or α particles, and <1% heavier nuclei[2,21,22,23]. For the 97.73% confidence case shown in Figure 10, the percent contribution of H is 99.73% and the percent contribution of He is 0.0488%. When confidence is decreased to 50%, the percent contribution by H only decreases to 99.71%. Mrigakshi et al.[23] claimed ISO 15390, which models data obtained by the Advanced Composition Explorer, overestimates H flux by 40-70% and He flux by 25-40%. This work supports the findings of Mrigakshi et al., and mission designers may wish to apply a factor of 0.3.

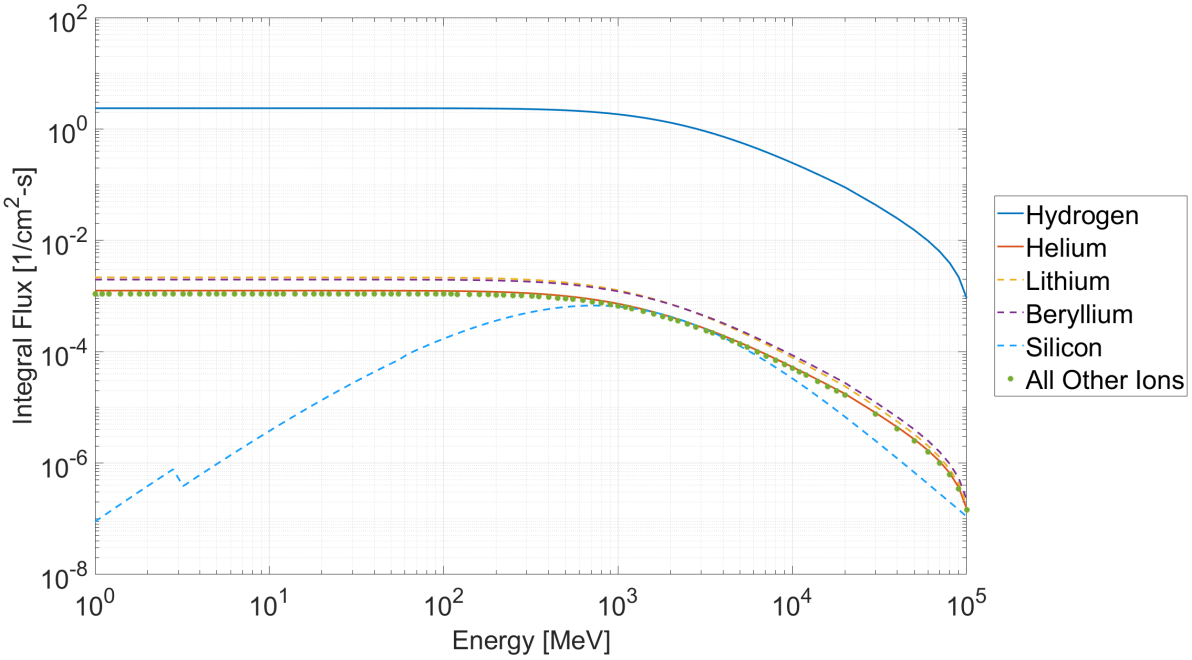

Figure 9: GCR Integral Flux vs. Energy by Species, ISO 15390, 97.73% Confidence, Magnetospheric Shielding Off, Solar Maximum, Oct 1 2024 – Sep 30 2025

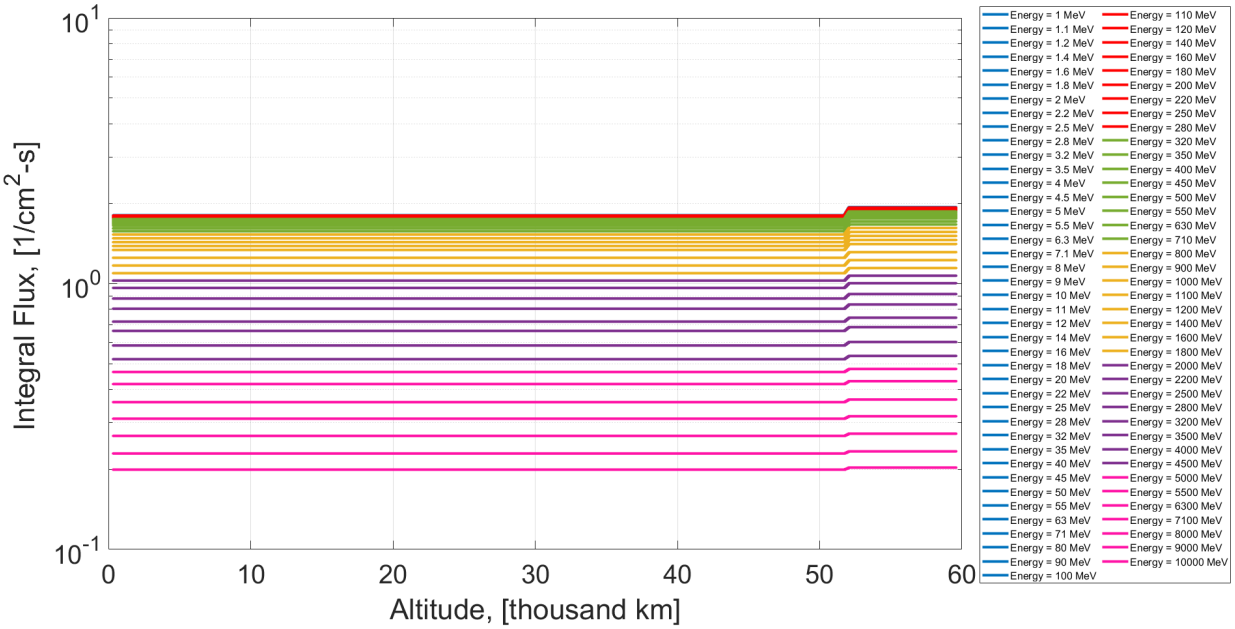

Figure 10: GCR Hydrogen and α-Particle Integral Flux vs. Altitude, ISO 15390, 97.73% Confidence, Magnetospheric Shielding On Below 52,000 km, Solar Maximum, Oct 1 2024 – Sep 30 2025

TOTAL IONIZING DOSE

Imparted dose from ionizing radiation is the most pertinent consideration for ABEX component selection. TID analyses are performed using the Multi-Layered Shielding Simulation (MULASSIS) within SPENVIS[24]. MULASSIS simulates radiation transport and incident particle interaction in multi-layered, one-dimensional shielding. MULASSIS contains a library of pre-defined materials as well as the option for user-defined materials.

It is convenient to associate a given shielding material thickness, aluminum 6061-T6 in the present work, with TID in an electronic component, here represented as a silicon wafer of thickness 0.25 mm. Silicon wafer thickness sensitivity testing was performed and found that silicon thickness did not appreciably affect TID results. Radiation sources in the TID assessment included VAB trapped electrons, VAB trapped protons, SEP protons, GCR protons, and GCR alpha particles. Aluminum shielding thicknesses varied from 1 mm to 20 mm, and TID in the silicon wafer was calculated for each aluminum thickness for each radiation source and then summed. One term power law fits were determined for each particle source and the total with R^2 values above 0.995. Fits for TID in an electronic component are provided for VAB trapped electrons in Eq.(1), VAB trapped protons in Eq.(2), SEP protons in Eq.(3), GCR protons in Eq.(4), and a summed total in Eq.(5). The fits may underestimate TID because SEP only includes proton contributions and GCR only includes proton and alpha particle contributions, but both SEP and GCR are for the +2σ confidence levels. Applying a 10-20% margin to any TID assessment should account for worst-case underestimations. Eqs.(1-5) are specific to the ABEX orbit for a duration of 1 year. TID is in units of rads. Thickness is in units of mm.

$$TID_{VAB,e} = 102500 \cdot t_{shield}^{-2.320} \quad (1)$$

$$TID_{VAB,p} = 15290 \cdot t_{shield}^{-1.727} \quad (2)$$

$$TID_{SEP,p} = 33.84 \cdot t_{shield}^{-1.759} \quad (3)$$

$$TID_{GCR} = 5.059 \cdot t_{shield}^{0.1175} \quad (4)$$

$$TID_{Total} = 117900 \cdot t_{shield}^{-2.229} \quad (5)$$

Eqs.(1-5) should be used in the Phase A component selection process. Vendors provide the thickness of the outer component casing, which is commonly aluminum, and that thickness in mm is substituted into Eq.(5) to determine the total TID that material should expect to encounter. Mission designers and engineers wishing to use Eqs.(1-5) for a shorter duration than 1 year can apply fractions to yield their desired duration so long as the duration is within solar cycle 25.

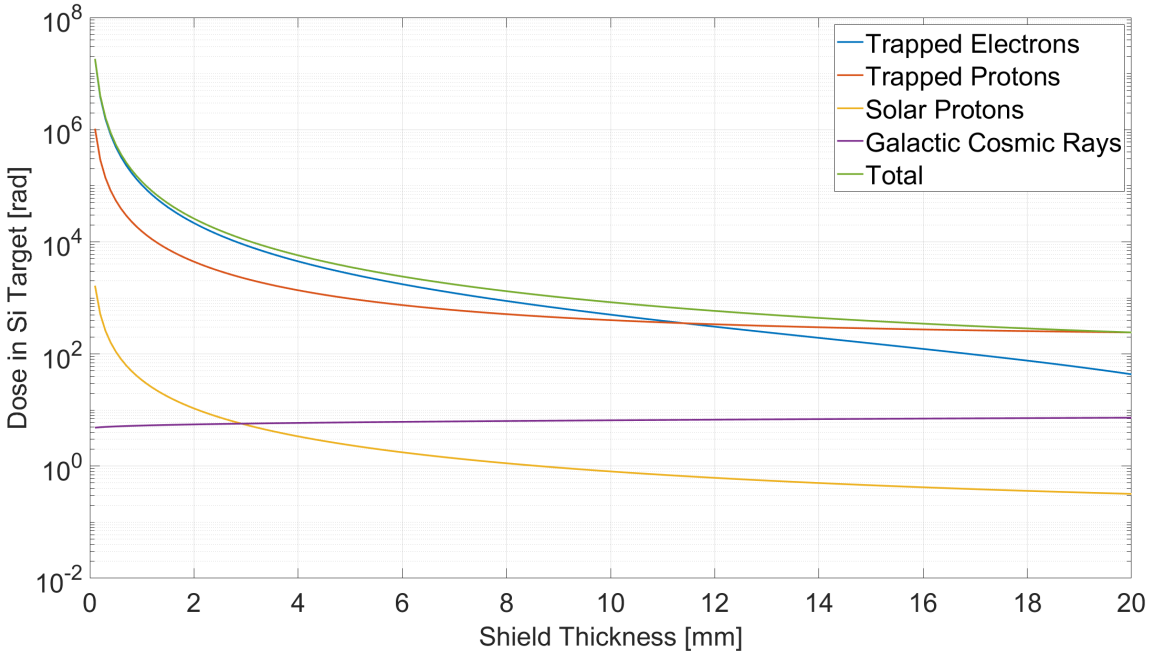

Figure 11: TID in 0.25 mm Si per Al Shielding Thickness, 97.73% Confidence, Magnetospheric Shielding Off, Oct 1 2024 – Sep 30 2025

NON-IONIZING ENERGY LOSS

Solar cell degradation results from the physical displacement of the solar cell's atomic lattice structure. This degradation is directly related to the Displacement Damage Dose (DDD) resulting from NIEL[25]. Whereas TID accounts for ionization and subsequent hole trapping, which can be caused by electrons, protons, ions, or energetic photons, DDD caused by NIEL is a metric of lattice damage. DDD is generally three-to-four orders of magnitude less than TID, a sensible consequence considering energetic particles are more likely to interact with lattice electrons than the lattice atoms themselves[2].

On-orbit degradation due to deleterious radiation occurs in solar cells, thermal coatings, battery cells, circuitry, and Charged Couple Devices, and adding shielding will reduce the degradation rate. Solar cell shielding is known as coverglass, and cells are commonly fabricated as Coverglass Interconnected Cells (CIC). The type and thickness of CIC coverglass determines the degradation rate, but missions with high solar cell number requirements may not have mass margin available for thick coverglass. The goal of NIEL characterization is to reduce cell efficiency degradation while minimizing mass requirements.

The ABEX mission equivalent fluence, solar cell DDD, and power degradation were simulated in SPENVIS using EQFLUX[26] and MC-SCREAM[27]. Inputs to EQFLUX include the solar cell type based on predefined suppliers and coverglass density and thickness; EQFLUX outputs solar cell equivalent fluence. MC-SCREAM inputs include cell equivalent fluence and NIEL-specific material parameters: C (a unitless constant), D_x (mass stopping power coefficient), and n representing the electron damage coefficient[25]. MC-SCREAM calculates DDD and solar cell power efficiency degradation. The combination of EQFLUX and MC-SCREAM allows for power degradation to be analyzed over different orbit durations with varying coverglass thickness values, yielding a normalized solar cell power efficiency sensitivity analysis against mass.

The ABEX solar cell is the Spectrolab XTE-HF cell[28], but parameters for the XTE-HF are not yet available in EQFLUX. Spectrolab's XTJ Prime was selected as it is the closest available cell type to the Spectrolab's XTE-HF; both cells are triple junction with a GaAs center layer.

The MC-SCREAM input for this analysis is shown in Tables 4 and 5. The center layer, the primary layer for power generation, is the limiting cell layer responsible for most of the solar cell efficiency degradation[29]. For these simulations, a Gallium Arsenide layer with a thickness of 2 microns, a coverglass density of 2.23 g/cm^3 representing a Borosilicate coverglass, and coverglass thicknesses of 275, 435, 665 and 855 microns were used. The SPENVIS default NIEL and stopping power parameters for GaAs were used which reflect a best fit for the spectrum of electron energies, as seen in Table 5, with a value of ~1.7 for n specific to P_{max}[30].

Table 4: CIC Parameter Inputs for MC-SCREAM

Cell Area [cm^2]	26.62
Coverglass Thickness [µm]	275, 435, 665, and 885
Coverglass Density [g/cm^3]	2.23
Layer Material	Gallium Arsenide
Layer Thickness [µm]	2

Table 5: NIEL Parameter Inputs for MC-SCREAM

NIEL Parameters					
	P_{max}	V_{OC}	I_{SC}	V_{pmax}	I_{pmax}
Proton Parameters					
C	0.2904	0.115	0.229	0.115	0.229
D_x	1.1000	1.15	2.52	1.15	2.52
Electron Parameters					
C	0.3630	0.0745	0.3430	0.0745	0.343
D_x	6.9000	1.2800	11.0000	1.28	11.0
n	1.6470	2.1280	1.3260	2.128	1.326

The objective is to determine required coverglass thickness to meet End of Life (EOL) power consumption requirements for a given mission, which is subjective to satellite subsystem design. Voltage biases in the ABEX science instrumentation will drift due to TID resulting in increased power demands near EOL, and thermal coatings will similarly degrade resulting in increased heater wattage requirements. ABEX has a tentative goal of 80% normalized cell efficiency after one year in orbit but changing component selections may alter this goal. Simulations were run with an orbit duration of one year with coverglass thicknesses of 275, 435, 665, and 885 microns. Coverglass thickness as a function of normalized solar cell efficiency is depicted in Figure 12. This result signifies ABEX will require a coverglass thickness of at least 275 microns to meet 80% power generation by EOL. Figure 13 describes the mass implications of this analysis based on number of solar cells for a given mission, and Eq.(6) represents the function polynomial fit for the 100 cell case.

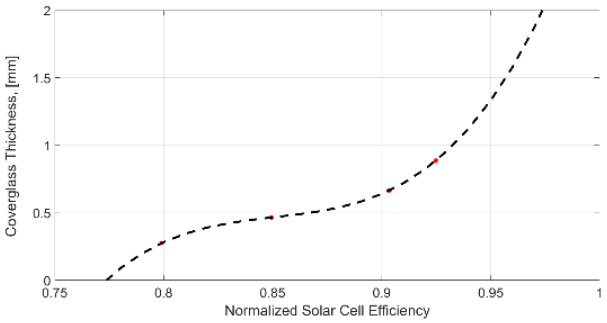

Figure 12: Normalized Solar Cell Efficiency vs. Coverglass Thickness, Borosilicate Coverglass, Spectrolab XTJ-Prime Cells, 1-Year Duration

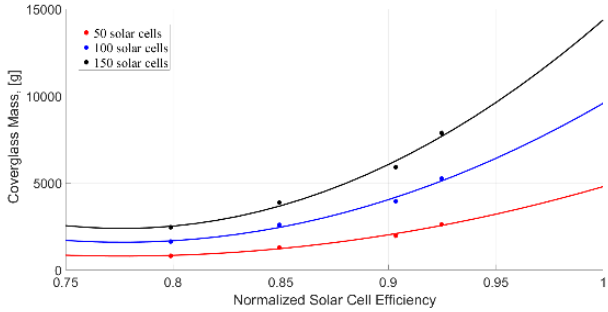

Figure 13: Normalized Solar Cell Efficiency vs. Mass, Borosilicate Coverglass, Spectrolab XTJ-Prime Cells, 1-Year Duration, Varied Cell Number

$$m_{cg} = 159{,}500 \cdot \eta_{Cell}^2 - 247{,}587 \cdot \eta_{Cell} + 97{,}672 \quad (6)$$

Eq.(6) signifies that if ABEX desires a cell efficiency η_{Cell} of 0.8 at EOL, a coverglass mass m_{cg} of 1,682.4 g covering 100 cells is required, or equally a coverglass mass of 16.824 g per cell. This trend may not be linearly applicable below cell efficiencies of 0.8 because the polynomial fit in Figure 12 declines sharply below 0.8, but Eq.(6) should be useful for η_{Cell} from 0.8 to 0.99.

Borosilicate was used for the purposes of this analysis because it is a common option from CIC manufacturers, but it is not the only option for cell coverglass material. If a program finds they need a mass-prohibitive borosilicate coverglass thickness to survive the intended environment, two options of merit are lead glass and fused silica. Lead glass is 1.39x denser than borosilicate but has mass attenuation coefficients orders of magnitude higher than borosilicate, meaning its specific transmittivity is much lower than borosilicate. Lead glass may darken when exposed to ionizing radiation. Fused silica is currently not produced at scale and may be cost-prohibitive, but it is colloquially referred to as SPF ∞ due to its extremely high NIEL resistance when used as CIC coverglass.

THERMAL SPACECRAFT ENVIRONMENT

Thermal Case Variation

Full SRE characterization is not complete without thermal analysis. Heat flux sources include direct solar radiation, Earth albedo radiation, Earth emission radiation, Free Molecular Heating (FMH), and CPH. Incident heat flux sources were categorized into cold case conditions, which are used to determine required heater wattage, hot case conditions, which are used to determine required radiator areas, and nominal trend conditions, which follow STK orbit data exactly. No assertions are provided about spacecraft temperatures, only incident heat fluxes. Heat fluxes are plotted per source for 2-week and 1-year periods. Parameter variations per case are discussed in source sections, and a parameter variation overview is provided in Table 6.

Direct Solar

The Sun is modeled as a blackbody at 5,780 K. Applying this temperature to Planck's blackbody equation and numerically integrating using the composite Simpson's 1/3 method yields a surface heat flux, $Q"_{Solar,Surf}$, of 62,943,984 W/m^2. Using a frontal patch-to-sphere radiative view factor[31], the variation of solar heat flux for a nominal trend case is described in Eq.(7).

$$Q"_{Solar} = \frac{Q"_{Solar,Surf}}{\left(\frac{D_{Sun}}{R_{Sun}}\right)^2} \cdot (1 - f_s) \quad (7)$$

D_{Sun} is the distance to the center of the Sun, R_{Sun} is radius of the Sun, and f_s is the shadow fraction. D_{Sun} is the varied parameter in the nominal trend case. Solar heat flux is 1,322 W/m^2 at aphelion and 1,414 W/m^2 at perihelion with less than 1% variation between solar minima and maxima[5,7]. The values have been verified within 0.4% by the World Radiation Center in Davos, Switzerland[32,33]. Direct solar heat flux for 2-week and 1-year periods are shown in Figures 14 and 15. Shadow fraction f_s was provided from the STK trajectory model.

Figure 14 displays the consequence of total or partial eclipse for heat flux calculations. The first partial eclipse in Figure 14 lasts ~155 minutes, the second lasts ~360 minutes, and the full eclipses last between 15 and 25 minutes on average. Visible in Figure 15 is the variation of nominal trend case heat flux over time compared to the static nature of hot and cold case heat flux. Hot and cold case values do not change based on STK-generated altitudes, but the trend case does.

Table 6: Cold, Nominal Trend, and Hot Case Parameter Variation

Heating Type	Parameter	Cold Case	Trend Case	Hot Case
Direct Solar	Distance to Sun Center	~152,000,000 km	Variable	~147,000,000 km
Earth Emission[5]	Earth blackbody temperature	252.96 K	255.15 K	261.34 K
Earth Albedo[5]	Albedo factor, Distance to Sun Center	0.3	0.33	0.35
Free Molecular[5]	Atmospheric density	$2.72 \cdot 10^{-19}$ kg/m^3	Variable	$2.27 \cdot 10^{-11}$ kg/m^3
Trapped Electrons (CPH)	Particle flux concentration via confidence level	50%	84.1%	97.73%
Trapped Protons (CPH)	No hot/cold case	N/A	Solar maximum	N/A
Solar Energetic Particles (CPH)	Particle flux concentration	50%	84.1%	97.73%

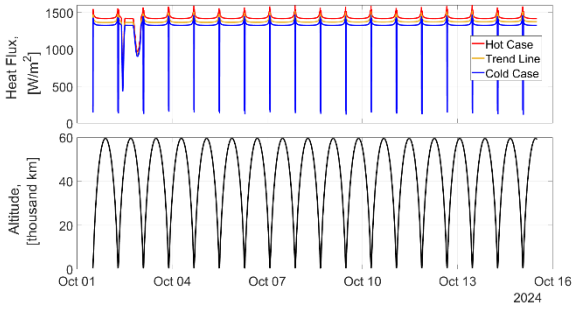

Figure 14: Incident Direct Solar Heat Flux, All Cases, Two Weeks, Oct 1 2024 – Oct 14 2024

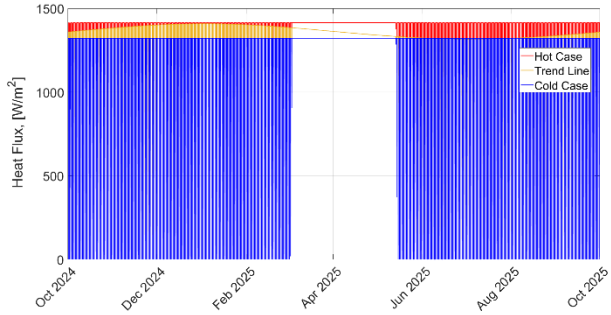

Figure 15: Incident Direct Solar Heat Flux, All Cases, One Year, Oct 1 2024 – Sep 30 2025

Planetary Albedo

Planetary albedo results from direct solar radiation reflecting off a planetary body and is practically dependent upon planetary spherical albedo if outside Low Earth Orbit (LEO) or, ideally, location-specific albedo if inside LEO. Invariant planetary spherical albedo factors were used for this analysis wherein 0.3, 0.33, and 0.35 were considered the cold, nominal trend, and hot case albedo factors[5]. Albedo is also dependent upon solar zenith angle, ξ. A spacecraft directly between the Sun and Earth would experience $\xi = 0°$, and albedo is only present when ξ is between 90° and -90°. To reiterate, albedo radiation is zero both during eclipse and when the magnitude of ξ is greater than 90°, not only during eclipse. Albedo heat flux is calculated by Eq.(8), where D_{Orbit} is the altitude of the CubeSat, R_{Earth} is the radius of the Earth, aF is the albedo factor of the Earth, and ξ is the solar zenith angle, or the angle between the satellite and orbit noon.

$$Q"_{Albedo} = \frac{Q"_{Solar}}{\left(\frac{D_{Orbit}+R_{Earth}}{R_{Earth}}\right)^2} \cdot aF \cdot \cos(\xi) \cdot (1 - f_s) \quad (8)$$

The cosine of the solar zenith angle ($0° \leq |\xi| \leq 180°$) can be calculated using the Eq.(9), where $\vec{V}_{E,cs}$ is the vector from the Earth to the CubeSat and $\vec{V}_{E,S}$ is the vector from the Earth to the Sun.

$$\cos(\xi) = \frac{\vec{V}_{E,cs} \cdot \vec{V}_{E,S}}{|\vec{V}_{E,cs}| \cdot |\vec{V}_{E,S}|} \quad (9)$$

The calculated heat flux is the incident heat flux, and it should not be considered the exact heat flux a satellite would experience because it does not account for the radiative view factors of multiple spacecraft faces. Albedo or Earth emission incident heat flux may apply appreciably to multiple spacecraft faces at sufficiently low Earth altitudes. Radiative view factors must be applied to all relevant faces[31]; Rickman[6] applies albedo heat flux to the nadir face of a nadir-pointed CubeSat in his analysis but only applies albedo heat flux to two of the four tangent faces in the nadir configuration. A thorough albedo flux application would involve 5 faces of a nadir-pointed spacecraft. This consideration equally applies to Earth emissive radiation.

Results for Earth albedo heat flux over the 2-week and 1-year orbit periods are shown in Figures 16 and 17, respectively. Albedo heat flux increases as the satellite approaches perigee, shown by the heat flux spikes at lower altitudes, but eclipse also occurs near perigee for the early mission months. As the argument of perigee shifts over time, eclipse no longer occurs during local albedo flux maximum, and albedo flux becomes significant.

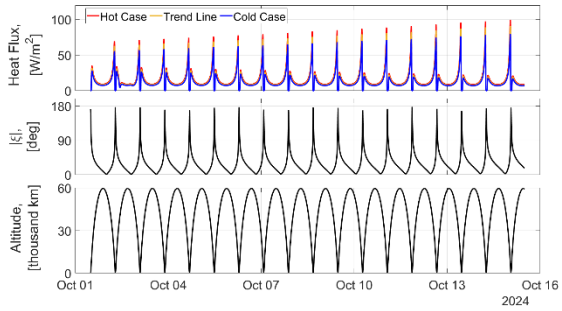

Figure 16: Incident Earth Albedo Heat Flux, All Cases, Two Weeks, Oct 1 2024 – Oct 14 2024

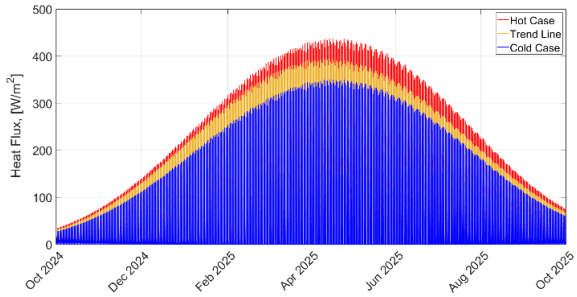

Figure 17: Incident Earth Albedo Heat Flux, All Cases, One Year, Oct 1 2024 – Sep 30 2025

Planetary Emission

Like direct solar heat flux, planetary emissive heat flux can be calculated by applying a temperature to Planck's blackbody equation. The cold case temperature is 252.96 K, the hot case temperature is 261.34 K, and the nominal trend is considered 255.15 K; these temperatures are 24-hour average measurements that are back calculated using measurements of Earth's emissivity[5]. A single blackbody temperature for Earth is a bad assumption in LEO just as a single albedo factor is a bad assumption. Because ABEX spends only 25 minutes below 1,600 km, the impact of these poor assumptions is considered manageable. Eq.(10) calculates incident planetary emissive heat flux.

$$Q"_{Emission} = \frac{Q"_{Earth,Surf}}{\left(\frac{D_{Orbit}+R_{Earth}}{R_{Earth}}\right)^2} \quad (10)$$

$Q"_{Earth,Surf}$ is the total heat flux emitted from the Earth at Earth's surface equaling 252.8 W/m^2 for the hot case, 221.0 W/m^2 for the cold case, and 229.0 for the trend case. Results for Earth emission heat flux over 2-week and 1-year orbits are shown in Figures 18 and 19, respectively. The heat flux increases as the satellite approaches perigee, shown by the heat flux spikes at lower altitudes.

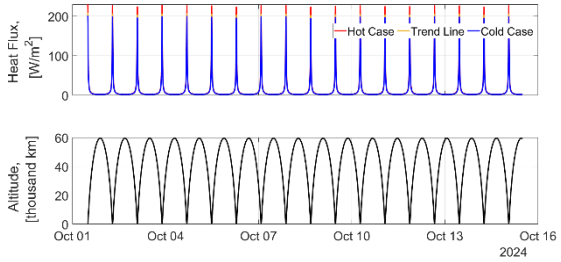

Figure 18: Incident Earth Emission Heat Flux, All Cases, Two Weeks, Oct 1 2024 – Oct 14 2024

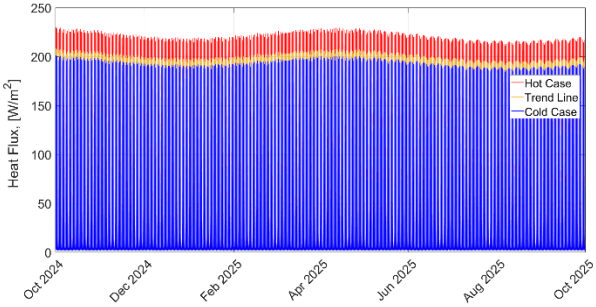

Figure 19: Incident Earth Emission Heat Flux, All Cases, One Year, Oct 1 2024 – Sep 30 2025

Free Molecular Heating

FMH is caused by atmospheric drag where spacecraft traveling at high velocities collide with particles in the upper atmosphere. These collisions, dependent on spacecraft velocity and atmospheric density, transfer kinetic energy to the spacecraft surface that is converted to heat. Orbital velocities are provided from the STK model or calculated using the Vis-Viva equation. Atmospheric density is obtained using the NRLMSISE-00 model[34].Eq.(11) is used to calculate FMH[5].

$$Q''_{FMH} = \alpha_t \cdot \left(\frac{1}{2}\right) \cdot \rho_{atm} \cdot V^3 \tag{11}$$

Here, α_t is the thermal accommodation coefficient, ρ_{atm} is the atmospheric density, and V is the satellite velocity. The thermal accommodation coefficient relates to the energy conversion process occurring during the particle-craft collision and is represented as a ratio. For conservatism, the accommodation coefficient is taken to be unity. The hot case corresponds to the maximum expected atmospheric density for the orbit and the cold case the is minimum. The trend case is calculated from the NRLMSISE-00 model per satellite orbit position.

Results for FMH over the 2-week and 1-year orbit are shown in Figures 20 and 21, respectively. The atmospheric density is largest at perigee, so the FMH heating will be largest at lower altitudes. FMH is applied to the ram face and is not isotropic; no distinctions are made in heat flux figures about directionality.

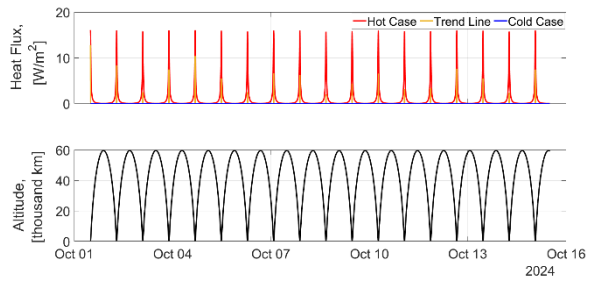

Figure 20: Incident Free Molecular Heat Flux, All Cases, Two Weeks, Oct 1 2024 – Oct 14 2024

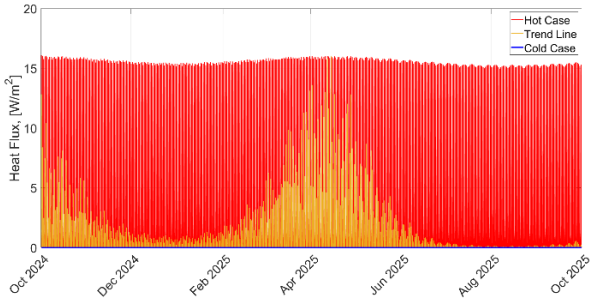

Figure 21: Incident Free Molecular Heat Flux, All Cases, One Year, Oct 1 2024 – Sep 30 2025

Charged Particle Heating Overview

Charged particle heating occurs when a spacecraft surface encounters energetic charged particles, meaning electrons, protons, or heavy ions mostly from VAB trapped particles or SEPs, which deposit energy to the spacecraft surface as a thermal load. Free neutrons are not commonly present in space unless produced nearby due to their half-life of 887.7 ± 2.2 seconds or 878.5 ± 0.8 seconds depending on how it is measured[35,36]. CPH calculations are presented in two steps that may be combined once understood. First, a specific power is determined by multiplying the stopping power, $\left(\frac{dE}{ds_{pen}}\right)_E$, which is a function of the target material and particle type for a given energy and has units of MeV-cm^2/kg, by the integral particle intensity, $\varphi(t,x)_E$, matching the particle type and energy level of the stopping power and having units of 1/cm^2-s-sr. As VAB trapped particle and SEP incidence is locally isotropic, a solid angle of 4π is applied to remove the steradian. A conversion factor, $K_E = 1.602 \cdot 10^{-13}$ J/MeV, converts MeV to J. This multiplication is shown in Eq.(12) and has units of W/kg.

$$Q'_{sp} = 4 \cdot \pi \cdot K_E \cdot \sum_{E_{min}}^{E_{max}} \left[\left(\frac{dE}{ds_{pen}}\right)_E \cdot \varphi(t,x)_E\right] \tag{12}$$

This specific power is a function of particle energy, stopping power, and particle intensity. The particle energy, E, is measured in MeV and represents the energy level associated with the type of particle that interacts with the spacecraft surface. The stopping power, $\left(\frac{dE}{ds_{pen}}\right)_E$, is an opposing force acting on the particle when it collides and penetrates the spacecraft surface which results in a loss of particle energy. Stopping power values are collected from lookup tables provided by NIST[37,38,39]. These tables are available for electrons, protons, and alpha particles with energies ranging from 0.001 MeV to 10,000 MeV. The particle integral intensity, $\varphi(t,x)_E$, represents the number of particles that cross a control area for some unit time step for a given solid angle and can be generated in SPENVIS. Using those stopping power values from NIST, particle penetration depth is calculated using the target material density and the associated particle energy per Eq.(13).

$$s_{pen} = \frac{E}{\left(\frac{dE}{ds_{pen}}\right)_E \cdot \rho_{mat}} \tag{13}$$

To obtain heat flux units of W/m^2 one can multiply Q'_{sp} by the surface material density and particle penetration depth, which for ABEX purposes did not exceed 20 mm Al. The material density, ρ_{mat}, is in units of kg/m^3, and penetration depth, s_{pen}, is in units of m. An expression

for CPH heat flux from this methodology is shown in Eq.(14) with units of W/m^2.

$$Q''_{CPH} = Q'_{sp} \cdot \rho_{mat} \cdot s_{pen} \quad (14)$$

A confidence interval of 97.73% was used to model the hot case particle intensity, $\varphi(t,x)_E$; confidence intervals for trend and cold cases were 84.1% and 50%, respectively.

VAB Trapped Proton CPH

The results for the trapped proton heat flux over the 2-week and year-long orbit are shown in Figures 22 and 23, respectively. Trapped protons are primarily present in the inner VAB. AP8 does not utilize confidence intervals so no case variation is provided.

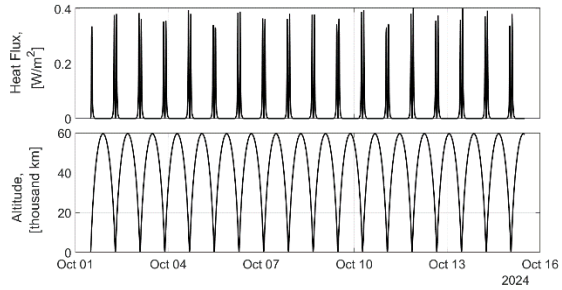

Figure 22: Incident Trapped Proton CPH Flux, Solar Maximum Case, Two Weeks, Oct 1 2024 – Oct 14 2024

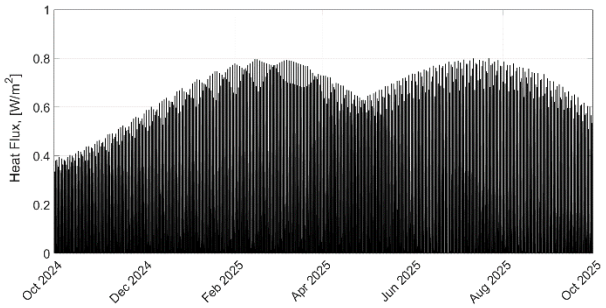

Figure 23: Incident Trapped Proton CPH Flux, Solar Maximum Case, One Year, Oct 1 2024 – Sep 30 2025

VAB Trapped Electron CPH

Results for trapped electron heat flux over the 2-week and 1-year orbit are shown in Figures 24 and 25, respectively. Trapped electrons are primarily present in the outer VAB. VAB electron CPH is approximately double VAB proton CPH, but all VAB CPH is functionally negligible compared to direct solar heat flux.

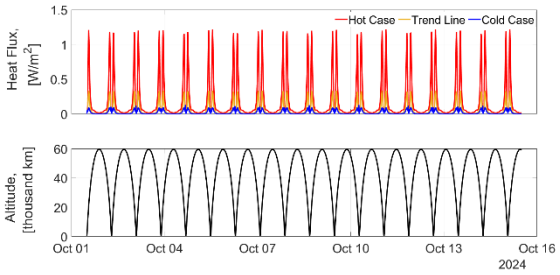

Figure 24: Incident Trapped Electron CPH Flux, All Cases, Two Weeks, Oct 1 2024 – Oct 14 2024

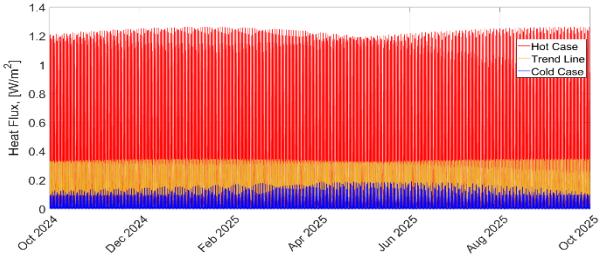

Figure 25: Incident Trapped Electron CPH Flux, All Cases, One Year, Oct 1 2024 – Sep 30 2025

SEP CPH

A CME occurrence probability of 42 CMEs per year was determined from solar cycle 23 analysis, described in the Sun Conditions section. Each CME is assumed to increase proton incidence for 12 hours. The numerical thermal model features a time step, and the probability of a CME occurring at each time step can be assessed. Eq.(15) calculates the probability of a CME occurring at a given time step; multiple CMEs may occur within a 12-hour period and cumulatively overlap.

$$P(CME) = n_{CME} \cdot K_t \cdot \Delta t \quad (15)$$

Parameter n_{CME} is the predicted number of CMEs per year, K_t is a conversion factor from years to minutes, and Δt is the time step interval, in minutes. For 42 CMEs per year and a time step of 5 minutes, the probability of a CME occurring in the model is 0.00039954 CMEs per time step. Quiet Sun particle flux conditions are used when no CME is present. Both CME and quiet Sun conditions exhibit distinct fluxes based on if ABEX is above or below 52,000 km (magnetically shielded or not, the threshold is somewhat arbitrary); blank data is used for eclipse condition particle flux. Five levels of SEP CPH are possible: eclipse, quiet Sun with and without magnetospheric shielding, and CME conditions with and without magnetospheric shielding. Results for SEP heat flux over the 2-week and 1-year orbit are shown in Figures 26 and 27, respectively. Since CME origination is probabilistic, the date that these heat flux spikes occur will vary each time the thermal model is executed. The number of CMEs will remain roughly ~42 CMEs/year.

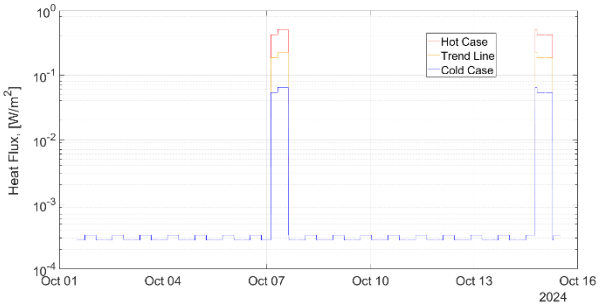

Figure 26: Incident SEP CPH Flux, All Cases, Two Weeks, Oct 1 2024 – Oct 14 2024

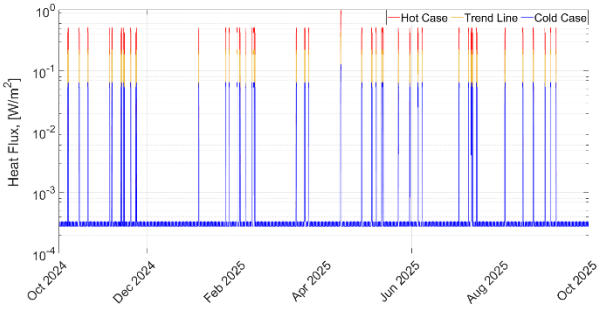

Figure 27: Incident SEP CPH Flux, All Cases, One Year, Oct 1 2024 – Sep 30 2025

Total Heat Flux Environment

The total incident heat flux was calculated by summing each heat flux instantaneously at all time steps at any time or position of interest in orbit. Total heat flux is summed in Eq.(16).

$$Q''_{total} = Q"_{Solar} + Q"_{Albedo} + Q"_{Emission} + Q''_{FMH} + Q''_{CPH} \quad (16)$$

Applying hot, cold, and nominal trend heat flux definitions to spacecraft areas, emissivities, absorptivities, and values adjustments for EOL allows for best, first, worst, and last spacecraft responses to space radiation environments. The relative contribution of thermal space radiation sources over two weeks is shown logarithmically in Figure 28 where eclipse conditions are represented as blank data points. Probabilistic CMEs are visible in Figure 28. This data is shown for a full year in Figure 29, and a linear version is provided in Figure 30 with attention paid to total values in lieu of relative contributions. The total heat flux for the logarithmic data visualization in Figure 29 tracks direct solar almost exactly due to the relatively low contribution from other sources and is not given a distinct line. The small dips in direct solar represent partial eclipses; total eclipses are not represented in log scale because they are zeroes.

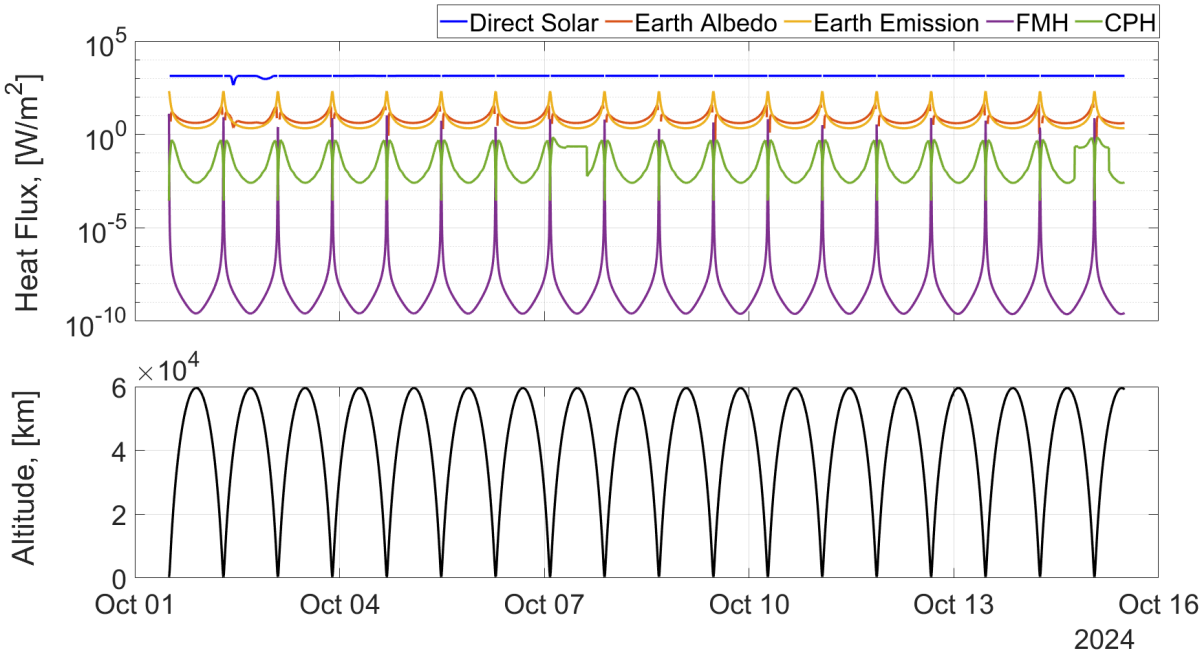

Figure 28: Incident Heat Flux from All Sources, Trend Case, Two Weeks, Oct 1 2024 – Oct 14 2024

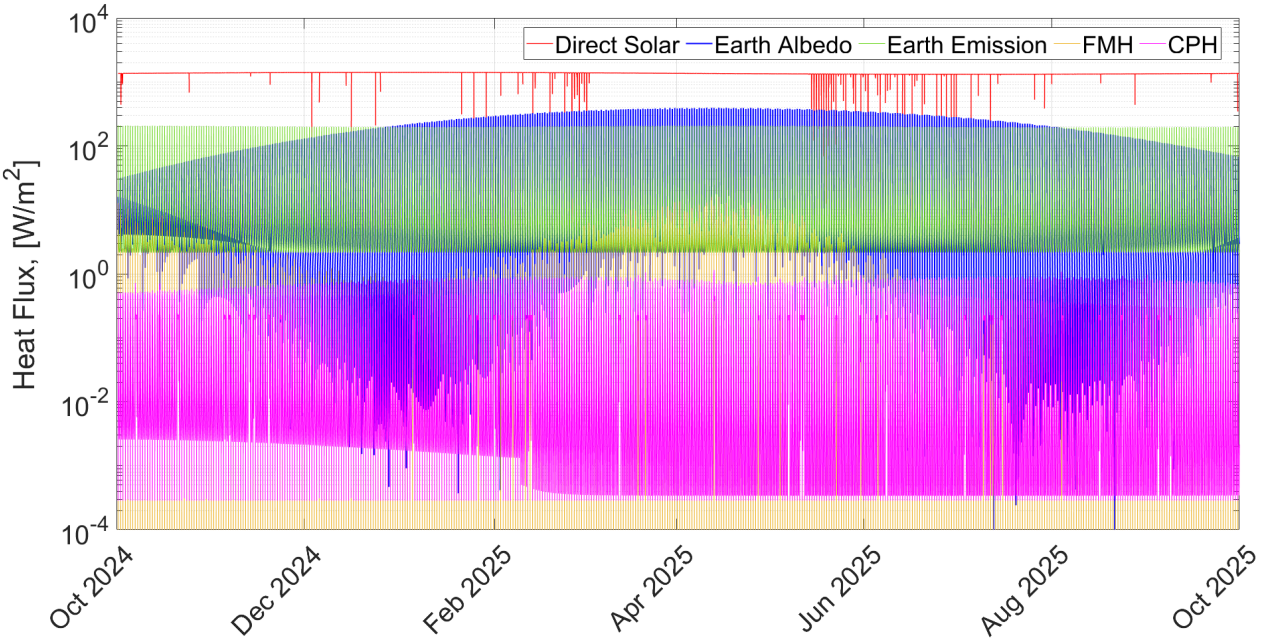

Figure 29: Incident Heat Flux from All Sources, Trend Case, One Year, Oct 1 2024 – Sep 30 2025

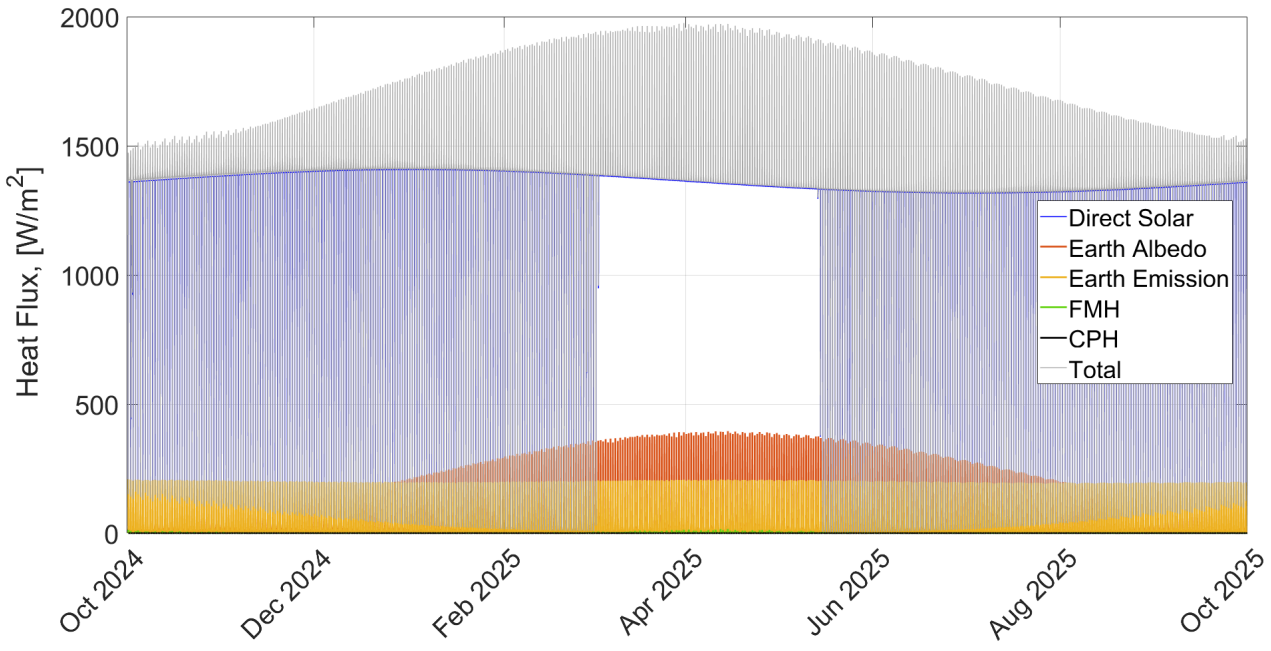

Figure 30: Total Incident Heat Flux from All Sources, Trend Case, One Year, Oct 1 2024 – Sep 30 2025

CONCLUSION

The ABEX radiation team has modeled the Space Radiation Environment for solar cycle 25 with attention paid to worst-case spacecraft thermal environment scenarios. VAB particles were found to be the highest contributor to TID, and a flux-based boundary to the outer VAB was set to 52,000 km. CMEs were found to raise proton flux levels by at least three-to-four orders of magnitude for all energy levels. A total of 42 CMEs are predicted to impact ABEX during the mission epoch of Oct 1 2024 to Sep 30 2025; prediction of CMEs months in advance may be possible by modeling solar system barycenter jerk maxima. CPH was deemed not to have an appreciable thermal effect compared to direct solar radiation, Earth albedo, or Earth emission. Particle flux is not negligible outside of CPH purposes as high proton flux CMEs and high energy GCR will cause SEEs, increased TID, increased NIEL, and surface charging effects. Silicon was the only outlier in particle flux behavior under 1 MeV for SEPs and 1,000 MeV for GCR, which may be a result of model inconsistencies or lack of empirical data. An aluminum shielding thickness of 3 mm was shown to keep circuitry TID below 10,000 rads over the full mission epoch. A solar cell coverglass thickness of 275 microns with a mass of 16.824 g per cell was found to reduce normalized solar cell efficiency loss to 20% over a year for the ABEX radiation environment. In non-normalized terms, a solar cell with an efficiency of 32.1% would have an efficiency of 0.2568 after a year.

Acknowledgments

ABEX would like to thank the ASGC for its continued support, specifically Dr. L. Dale Thomas, Debora Nielson, and Brooke Graham. ABEX thanks its Subject Matter Experts, Stephanie Mauro at MSFC, Dr. Dan Harris at Auburn, Dr. Qiang Hu at UAH, and Director of the Science and Technology Institute Dr. Linda Parker. Finally, ABEX thanks and acknowledges the undergraduate orbit team students at Auburn for generating the STK input data for this analysis.

References

1. Fuchs, Jared. Halvorson, Michael. Lopez, Victor "An Overview of the Alabama Burst Energetics Explorer Mission," Proceedings of the Small Satellite Conference 2021, Next on the Pad, WK-II. <URL to be published>.

2. Nöldeke Christoph M. The Space Radiation Environment. Monsenstein Und Vannerdat, 2015

3. Cane, H. V. (2000). Coronal mass ejections and Forbush decreases. Space Science Reviews, 93(1–2), 55–77.

4. Mann, Ian Robert, et al. "Explaining the dynamics of the ultra-relativistic third Van Allen radiation belt." Nature Physics 12.10 (2016): 978-983.

5. Gilmore, David G., and Martin Donabedian. Spacecraft Thermal Control Handbook. American Institute

6. Rickman, Steven L. "Introduction to on-orbit thermal environments." Thermal and Fluids Analysis Workshop. 2014.

7. Halvorson, Michael. "On the Design, Synthesis, and Radiation Effect Prevention of a 6U Deep Space CubeSat"

8. Garner, Rob. "Solar Storm and Space Weather - Frequently Asked Questions." NASA, NASA, 19 Mar. 2015, www.nasa.gov/mission_pages/sunearth/spaceweather/index.html#q2.

9. Potter, Sean. "Solar Cycle 25 Is Here. NASA, NOAA Scientists Explain What That Means." NASA, NASA, 15 Sept. 2020, www.nasa.gov/press-release/solar-cycle-25-is-here-nasa-noaa-scientists-explain-what-that-means

10. Schrijver, Carolus J., et al. "The 2011 February 15 X2 flare, ribbons, coronal front, and mass ejection: interpreting the three-dimensional views from the solar dynamics observatory and STEREO guided by magnetohydrodynamic flux-rope modeling." The Astrophysical Journal 738.2 (2011): 167.

11. "Coronal Mass Ejections." Coronal Mass Ejections | NOAA / NWS Space Weather Prediction Center, www.swpc.noaa.gov/phenomena/coronal-mass-ejections.

12. Maker, David. Email Correspondence. 31 May 2021.

13. Anagnostopoulos, G., et al. "The sun as a significant agent provoking earthquakes." The European Physical Journal Special Topics 230.1 (2021): 287-333.

14. Jordan, Carolyn E. NASA radiation belt models AP-8 and AE-8. RADEX INC BEDFORD MA, 1989.

15. Zell, Holly. "Radiation Belts with Satellites." NASA, NASA, 23 Mar. 2015, www.nasa.gov/mission_pages/sunearth/news/gallery/20130228-radiationbelts.html.

16. Johnston, W. Robert, et al. "AE9/AP9/SPM: New models for radiation belt and space plasma specification." Sensors and Systems for Space Applications VII. Vol. 9085. International Society for Optics and Photonics, 2014.

17. "AE9/AP9/SPM: Radiation Belt and Space Plasma Specification Models Air Force Research Laboratory (AFRL)." AE9/AP9/SPM Factsheet, www.vdl.afrl.af.mil/programs/ae9ap9/factsheet.php

18. P. Jiggens et al., "The Solar Accumulated and Peak Proton and Heavy Ion Radiation Environment (SAPPHIRE) Model," in IEEE Transactions on Nuclear Science, vol. 65, no. 2, pp. 698-711, Feb. 2018, doi: 10.1109/TNS.2017.2786581.

19. Smith, E. J., et al. "The Sun and heliosphere at solar maximum." Science 302.5648 (2003): 1165-1169.

20. Devore, Jay L., et al. *Applied Statistics for Engineers and Scientists*. Duxbury, 2014.

21. Simpson, J. A. (1983), Elemental and isotopic composition of the galactic cosmic rays, Annu. Rev. Nucl. Part. Sci., 33, 323–382, doi:10.1146/ annurev.ns.33.120183.001543

22. Hörandel, J. R. (2008), The origin of galactic cosmic rays, Nucl. Instrum. Methods Phys. Res., Sect. A, 588, 181–188, doi:10.1016/j.nima.2008. 01.036.

23. Mrigakshi, Alankrita Isha, et al. "Assessment of galactic cosmic ray models." Journal of Geophysical Research: Space Physics 117.A8 (2012).

24. Lei, F., et al. "MULASSIS: A Geant4-based multilayered shielding simulation tool." IEEE Transactions on Nuclear Science 49.6 (2002): 2788-2793

25. Messenger, Scott, et al. "Model comparisons for space solar cell end-of-life calculations." 9th European Space Power Conference. Vol. 690. 2011.

26. Calders, Stijn, et al. "Modeling the space environment and its effects on spacecraft and astronauts using SPENVIS." 2018 SpaceOps Conference. 2018.

27. Taylor, S., et al. "Use of ESA's SPENVIS software to compare 'end of life'performance of solar cells using different analysis methods."

28. XTE-HF (High Fluence) Space Qualified Triple Junction Solar Cell. Spectrolab, www.spectrolab.com/photovoltaics/XTE-HF Data Sheet _12.23.19.pdf.

29. Sato, Shin-ichiro. "Degradation Modeling of InGaP/GaAs/Ge Triple-Junction Solar Cells Irradiated with Various-Energy Protons." *Solar Energy Materials and Solar Cells*, vol. 93, no. 6-7, June 2009, pp. 768–773., doi:https://www.sciencedirect.com/science/article/pii/S0927024808003140?casa_token=Szzeax5hlMAAAAAA:3DsEtO8uR7HEldC1NE9Gs420LbDAVfPjAIS1ClH4QSgZb-yx7bQjgVPPXoCWu-kJqDi_7av4QA.

30. Messenger, Scott R., et al. "Modeling solar cell degradation in space: A comparison of the NRL displacement damage dose and the JPL equivalent fluence approaches." Progress in Photovoltaics: Research and Applications 9.2 (2001): 103-121.

31. Martinez, Isidoro. "Radiative View Factors. 2013."

32. Howell, John R., et al. Thermal Radiation Heat Transfer. 6th ed., CRC Press, 2016.

33. Fröhlich, C., and R. W. Brusa. "Solar radiation and its variation in time." Solar Physics 74.1 (1981): 209-215.

34. Picone, J. M., et al. "NRLMSISE-00 empirical model of the atmosphere: Statistical comparisons and scientific issues." *Journal of Geophysical Research: Space Physics* 107.A12 (2002): SIA-15.

35. Ramram, Adam. "Programmatic Thermal Neutron Flux Calibration for Neutron Generators." (2020).

36. Vasiliev, Boris V. "Effect of Reactor Neutrinos on Beta-Decay." Journal of Modern Physics 11.01 (2020): 91

37. Seltzer, Stephen M., et al. "Stopping Powers and Range Tables for Protons." *Physical Measurement Laboratory*, physics.nist.gov/PhysRefData/Star/Text/PSTAR.html.

38. Seltzer, Stephen M., et al. "Stopping Powers and Range Tables for Electrons." *Physical Measurement Laboratory*, physics.nist.gov/PhysRefData/Star/Text/ESTAR.html.

39. Seltzer, Stephen M., et al. "Stopping Powers and Range Tables for Helium Ions." *Physical Measurement Laboratory*, physics.nist.gov/PhysRefData/Star/Text/ASTAR.html.